



TEMGYM Advanced – NanoMi lens characterisation

David Landers^a, Ian Clancy^a, Rafal E. Dunin-Borkowski^b, Dieter Weber^b, Andrew A. Stewart^{c,*}

^a Department of Physics, University of Limerick, Limerick, Munster, V94 T9PX, Ireland

^b Ernst Ruska-Centre for Microscopy and Spectroscopy with Electrons, Forschungszentrum Jülich, 52425 Jülich, Germany

^c Department of Chemistry, University College London, 20 Gordon St, London WC1H 0AJ, United Kingdom

ARTICLE INFO

Keywords:

Ray tracing
NanoMi
Parallelisation
Finite element method
Differential algebra
Aberration integral

ABSTRACT

A complete analysis including finite element method (FEM) calculation, focal length properties, and thirdorder geometric aberrations of the open-source electrostatic lens from the NanoMi project is presented. The analysis is carried out by the software TEMGYM Advanced, a free package developed to carry out ray-tracing and lens characterisation in Python. Previously TEMGYM Advanced has shown how to analyse the aberrations of analytical lens fields; this paper expands upon this work to demonstrate how to apply a suitable fitting method to discrete lens fields obtained via FEM methods so that the aberrations of real lens designs can be calculated. Each software platform used in this paper is freely available in the community and creates a free and viable alternative to commercial lens design packages.

1. Introduction

The Finite Element Method (FEM) was introduced into electron microscopy in 1972 (Munro, 1972) enabling the calculation of magnetic fields of complicated pole piece shapes and saturated lenses, and paving the way for electron microscopists to develop a rich set of tools to analyse the performance of real electron lens designs. In the following decades, advanced commercial software packages for electron lens design were developed (MEBS & EOD (Munro, 2011; Lencová and Zlámal, 2008)), and are capable of modelling fields of real electron optical lens designs using FEM, characterising their first-order properties (such as focal length & magnification) and calculating aberration coefficients. In addition, the commercial software COMSOL (2020) is also used to model the field of electron lens computer aided design (CAD) models, although it does not readily provide tools to analyse the aberration coefficients of a lens.

MEBS & EOD provide specific tools to analyse the first-order properties of lens designs and aberration coefficients, however in each case, access to the code and methods of their programme is prohibited, and if a user wishes to modify the commercial software for their own needs, they must wait for the developers to implement it first. Furthermore, electron lens designs are often proprietary and not openly shared, adding to the difficulty of developing and testing software that can design and characterise electron lenses in a free and open-source manner.

The field of electron microscopy has made strides to facilitate an

ecosystem of open software with community packages such as PyXem, LiberTEM & HyperSpy (Johnstone, 2019; Clausen, 2020; De La Peña, 2021); however, very few if any free packages exist that can perform electron ray tracing, lens design and characterisation. Our software entitled TEMGYM Advanced (Landers et al., 2023) aims to fill this niche, and previously showed how to calculate aberrations and trace electrons through a series of theoretical electron microscope components in real-time.

This works aims to enable development of a digital twin electron microscope that can explore real-time automated control, a long sought-after goal (Tejada et al., 2011; Tejada et al., 2013; Koster and de Ruijter, 1992) that has re-entered discussion within the community (Dyck et al., 2019; Spurgeon, 2020), helped in part by the advent of machine learning control routines that have improved the standard of automated control tasks within a wide variety of fields (Wurman, 2022; Bellemare, 2020; Vinyals, 2019; Degrave, 2022). (Spurgeon, 2020) in particular note that the next generation of microscopes will require a new approach to experiment design, execution, analysis and data sharing. Thus, an open-source software package capable of characterising the performance and aberrations of microscope components and visualising the beam response inside the microscope in near-real time could be an important step towards achieving improved automation workflows. A number of groups have already made significant developments towards automated workflows in electron microscopy (Xu et al., 2022; Olszta; Kalinin, 2021; Rosi, 2022; Bertoni, 2023; Rotunno and Grillo, 2022;

* Corresponding author.

E-mail address: andy.stewart@ucl.ac.uk (A.A. Stewart).

Dupuy, 2021), and have already used basic digital-twin models of the electron microscope that can generate training data and enable offline exploration of automation routines, however often the important details of such a model are closed source. A further step that will enable the community to develop a digital twin further will be to have access to software that can characterise component performance openly, in a format that enables further integration with the de facto language for machine learning analysis, Python. The work presented in this paper uses access to the open-source electron microscope project entitled NanoMi (Malac et al., 2022), which openly shares its electrostatic lens designs, in combination with our ray tracing analysis software TEMGYM Advanced, to detail how to perform a complete characterisation of the first-order properties and third-order geometric aberration coefficients of a real electrostatic lens.

The first part of this paper begins with a calculation of the axial potential of the NanoMi lens CAD model via the open-source FEM package Finite Element Method Magnetics (FEMM) (Baltzis, 2008), and then shows how to apply the ray tracing package, TEMGYM Advanced, to the NanoMi lens, which solves the required equations of motion to characterise properties such as the focal length and aberrations of the lens. The software has been built using the Python programming language because of its accessibility and familiarity to scientists, who can now easily access the rich set of machine learning and optimisation routines in Python and leverage their capabilities to enable further exploration of instrument design and instrument automation.

2. FEM calculation

Finite Element Method Magnetics (FEMM) (Baltzis, 2008) is a finite element analysis software package used extensively for electromagnetic modelling tasks (Komárek and Klogner, 2022; Devi and Sanavullah, 2011) that comes with a rich Python interface enabling programmatic communication between Python & FEMM or the option to use an interactive GUI. FEMM only provides the ability to analyse 2D CAD models of a component; however, a 2D simulation of an electron lens design is all that is required, and indeed preferable to a 3D calculation, as a 2D simulation is much faster and requires far less random-access memory (RAM). Furthermore, only knowledge of the shape of the axial field, obtained from an axisymmetric 2D model, is required to calculate first-order properties and aberration coefficients up to n^{th} order in the case of round electron lenses (Szilagy, 1988; Hawkes and Kasper, 2017).

To model the NanoMi electrostatic lens, a cross-section of the NanoMi Lens CAD model is extracted using the online CAD software

OnShape (3D CAD Software & Product Development Platform, 2023), and it is converted to a .DXF file and input into FEMM. Then, after assigning a material to each region in the mesh, setting the problem to "axisymmetric" and applying a boundary condition, FEMM calculates the mesh using the open-source triangulation software, Triangle (Shewchuk, 1996) FEMM then solves the 2D Poisson equation to obtain the potential at the defined mesh points. Finally, the potential is extracted along the z-axis as a text file and input, into our Python scripts for pre-processing. Fig. 1.

3. NanoMi lens axial potential fit

The axial potential calculated by the finite element software FEMM is a set of discrete points describing the potential of the lens on the z-axis. It is necessary to cast the discrete potential into an analytical form to utilise this potential to trace rays through the lens and calculate aberrations via aberration integrals or the differential algebra method. The type of fitting procedure used is paramount, as to calculate third-order geometric aberration coefficients one needs to differentiate the axial lens potential four times. As a result, a traditional method such as cubic polynomial spline fitting, which only permits up to three derivatives, does not suffice. Three alternative methods that show how to obtain an analytical fit adequate for aberration analysis have been presented in the literature; (Wang, 2004) has shown how to use Hermite polynomials (Wang, 2004), K. Makino (Makino and Berz, 2006) have used a series of gaussian functions and (Kang et al., 2017) used a local quintic interpolation method. This work has opted to use a series of Gaussian functions fit to our potential via linear regression, utilising a function provided by the open-source package AstroPy (Robitaille, 2013). The advantage of the Gaussian fitting method is that one does not need to introduce a non-dimensional coordinate system, as (Wang, 2004) did to enable Hermite fitting of their potential. Furthermore, outside the range of the fit, the Gaussian function returns a value of zero, which is convenient as, far away from the lens, the potential tends toward zero.

The sum of Gaussian fitting method introduced by (Berz, 1989) also recommends that as many Gaussians as possible be fitted to the potential so that the error returned is minimal. For this work, the software uses the number of Gaussians, n , to be 201, but the exact value will need to be chosen on a case-by-case basis and will depend on the shape and length of the axial potential. Overfitting is not a concern in this case, because the fitted axial function should match as close as possible to the discrete axial potential returned by FEMM. Obtaining a functional representation of the axial field enables us to evaluate the electrostatic potential and its derivatives within the lens region to solve for the first-order properties

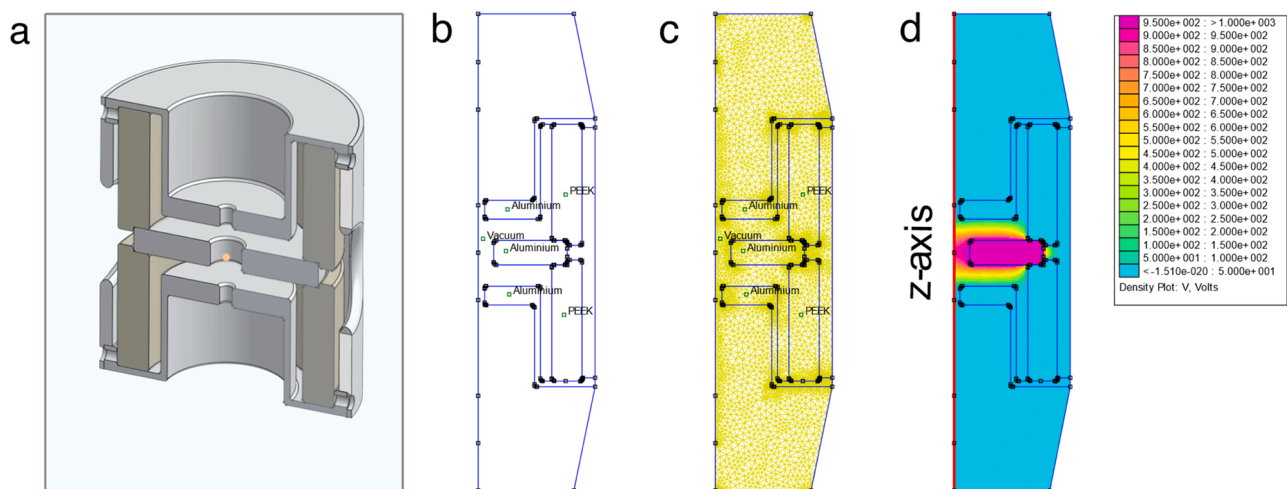


Fig. 1. Finite element calculation process of NanoMi lens. a) CAD model of NanoMi Lens as viewed in OnShape. b) Cross section of CAD model imported into FEMM, with appropriate materials designated. c) Triangulation of the 2D CAD drawing. d) Calculated potential surrounding the charged electrode.

and characterise the third-order geometric aberration coefficients, as shown in Fig. 2.

4. NanoMi lens focal length calculation via Linearised ODE equation

The first step to characterise the lens is to solve the linearised ordinary differential equation (ode) for an axisymmetric electrostatic axial potential (Szilagyi, 1988; Hawkes and Kasper, 2017; El-Kareh, 2012):

$$x'' + \frac{U'(z)}{2\phi}x' + \frac{U''(z)}{4\phi}x = 0 \quad (1)$$

$$y'' + \frac{U'(z)}{2U_0}y' + \frac{U''(z)}{4U_0}y = 0$$

where x, y and z are cartesian coordinates and $U(z)$ is the axial potential function of the lens. U_0 is the acceleration voltage of the electron, and primes denote differentiation w.r.t z . Primes denote derivatives w.r.t z . The generalised solution of Eq (1) is found by solving for two rays g & h with specific initial conditions of position and slope (see also (Szilagyi, 1988; Hawkes and Kasper, 2017; El-Kareh, 2012; Graef, 2003)):

$$g(z_0) = 1\text{m}, g'(z_0) = 0 \quad (2)$$

$$h(z_0) = 0\text{m}, h'(z_0) = 1$$

By solving the linearised equation of motion (Eq (1)) numerically for the initial conditions of the ray g with a position of 1m and slope of 0 in the object plane (blue ray in Fig. 3), one can obtain the focal length of the NanoMi electrostatic lens, and the magnification of the image in the image plane. By solving for the ray h , which begins with an initial radial position of 0m, and a slope of 1 in the object plane (red ray in Fig. 3), one calculates the location of the image plane. The g and h are generalised solutions to Eq (1) and, once known, can be readily used to calculate another ray path $p(z)$ with a different set of initial conditions.

$$p(z) = K_1g(z) + K_2h(z) \quad (3)$$

where K_1 is the initial radial position of at the object ($p(z_0)$), and K_2 is the initial slope of ($p'(z_0)$) at the object without solving the linearised equation again numerically. Furthermore, finding the principal rays g & h is also even more useful than just a first-order description of the beam path, as their slope and position form part of the solution of the aberration integrals to find the third-order aberration coefficients of the

lens, which is discussed in the section NanoMi Lens Aberration Coefficients. The linearised equation of motion implemented in our ray tracing code TEMGYM Advanced calculates the first-order optical properties of the NanoMi lens and verifies the accuracy of our FEM calculation by enabling us to compare our focal length results (determined by the axial potential calculated by the package FEMM) to those presented previously by (Malac et al., 2022; Rempfer, 1985). Malac et al. (2022) obtained their focal length results via a COMSOL simulation, & Rempfer (1985) calculated the focal length of this lens design experimentally using an optics table. Therefore, if our axial potential of the NanoMi lens calculated via FEMM is correct, the focal length calculated should agree with those presented by both Rempfer (1985) & Malac et al. (2022). The adaptive step RK54DP (Dormand and Prince, 1980; Dormand) method is used to solve the first-order ODE (Eq (1)); An adaptive step size method is very advantageous because there are large regions between the object and the image where the ray experiences no force from the lens, and thus a larger step size in those regions significantly speeds up the calculation. The traced rays (g & h) and their slope are fitted via a cubic spline polynomial, and then a root finding algorithm is used to obtain the focal length and Gaussian image plane after the lens. It is important to note that the ratio of the accelerating voltage of the electron over the accelerating voltage of the lens, U_1/U_0 determines the focal length of the lens. The lens potential is fixed at -1000V and U_0 is varied (also a negative value) to change the ratio U_1/U_0 .

Fig. 4 shows the asymptotic focal length results calculated using the linearised equation of electron motion and shows good agreement between our method and the focal length values calculated by Rempfer (1985) (experimental) & Malac et al. (2022) (COMSOL). The asymptotic focal length is found by connecting an asymptote from the ray after it has left the field of the lens and finding where that asymptote crosses the z -axis. This value can be different from the real focal length value if the real focal length is located inside the lens field, as the ray will continue to bend after this point due to the electric field (see Fig. 3). Furthermore, in the work presented by Malac et al. (2022), they state that they could not estimate the focal length below U_1/U_0 of 0.5, as their COMSOL simulation would fail. The software presented in this work can trace rays to any required length beyond the region of our lens field (which is 50 mm broad on either side of the lens), and thus can estimate the focal length values below a U_1/U_0 of 0.5. The method presented here is also quick and can calculate the 100 focal lengths shown in Fig. 4 in approximately 10 s.

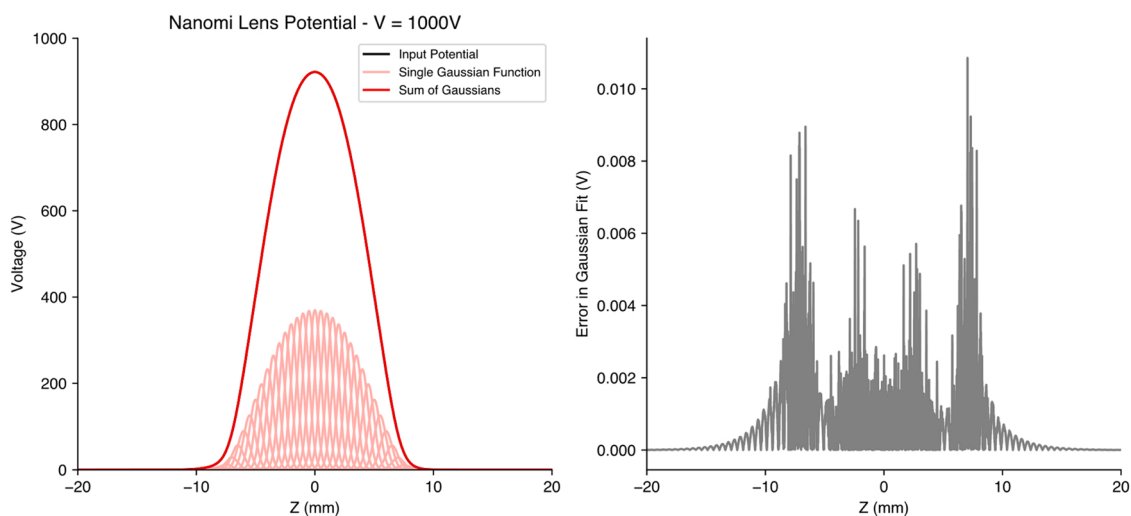


Fig. 2. Left Panel: Axial potential and Gaussian fitting method. The red line displays the sum of Gaussian function fit to the axial potential data (black, not visible), and the light red line displays each Gaussian used to obtain the fit. Right Panel: Absolute error in the fit between the axial potential obtained from the FEM method, and the sum of Gaussian fit.

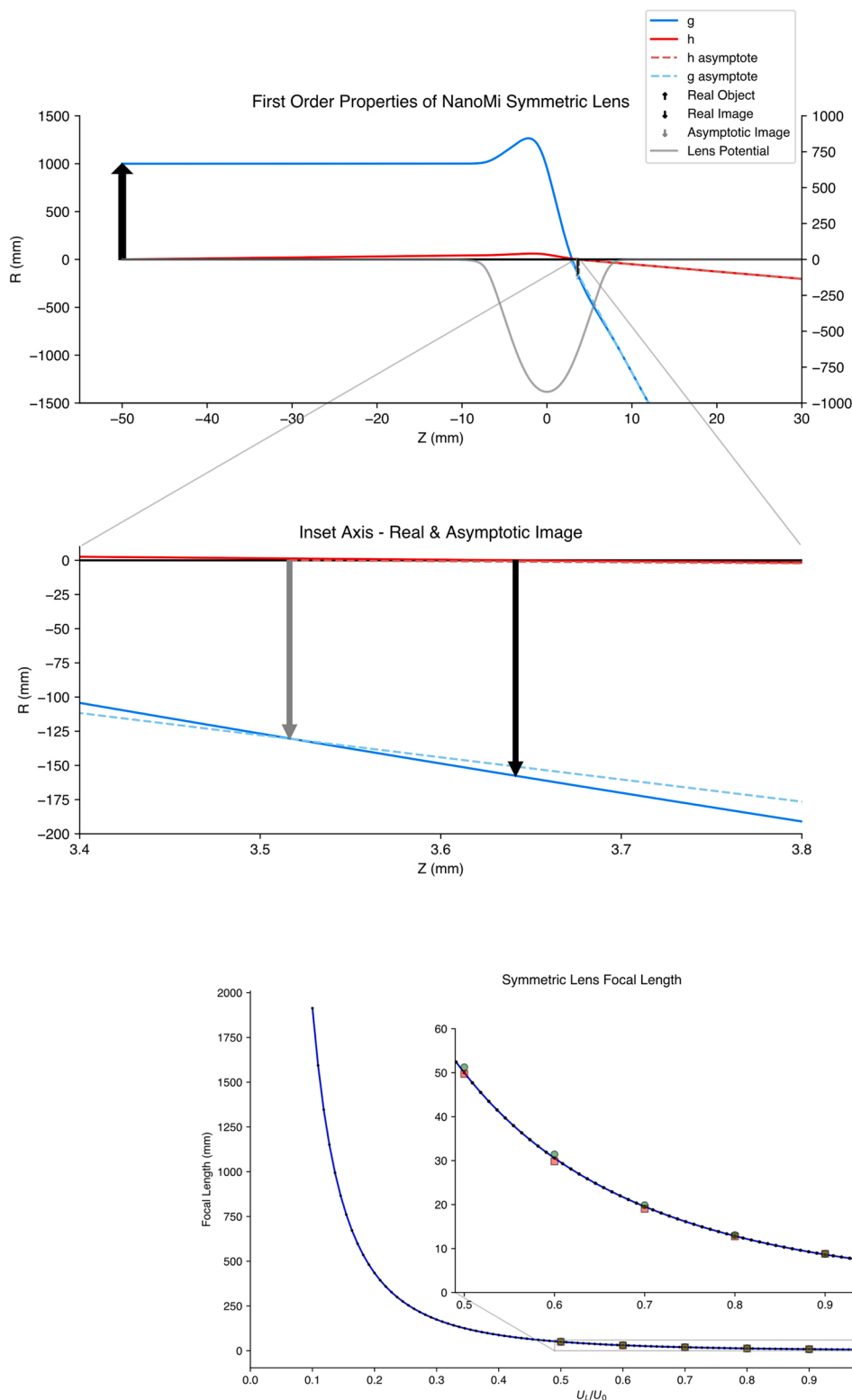


Fig. 3. Real & Asymptotic image formation. The top image shows the first-order ray solutions g and h obtained by solving the linearised ODE (Eq (1)). The bottom image shows a zoomed-in section of the image location, displaying the real and asymptotic image. The dashed blue and red lines are the asymptotes of the real ray paths (solid red and blue lines) of the principal rays g and h , obtained from the final slope of each ray, far after it has left the lens field. By tracing an asymptote back towards the lens from both rays, one can find where the virtual asymptotic image is formed, which also has its own corresponding set of aberration coefficients.

Fig. 4. Asymptotic focal length of NanoMi lens at varying voltage ratios U_1/U_0 .

5. NanoMi lens aberration coefficients

The tools developed in TEMGYM Advanced also enable calculation of the Real and Asymptotic third-order geometric aberration coefficients for the NanoMi Lens via the aberration integral method (Hawkes and Kasper, 2017) or the differential algebra (DA) method (Berz, 1989). Just as there exists a real and asymptotic focal length value if the lens forms

an image inside the field of the lens, real and asymptotic values also exist for the magnification & aberration coefficients. Again, the asymptotic variables are called as such because they are found by connecting an asymptote from the final slope of the ray back towards the lens. When the image and object are located outside the field of the lens, then the values of the real and asymptotic coefficients coincide, and one can use the differential algebra method or the real aberration integral method to

obtain the real aberration coefficients. See Fig. 3 for a graphical view that explains the meaning of real and asymptotic image formation.

To use the differential algebra method, one must first solve the trajectory equation of motion of the electron numerically (Szilagyi, 1988; Hawkes and Kasper, 2017):

$$x' = \frac{\rho^2}{2U_0}(E_x - x'E_z) \tag{4}$$

$$y' = \frac{\rho^2}{2U_0}(E_y - y'E_z)$$

with $\rho = \sqrt{1 + (x')^2 + (y')^2}$ and E_x, E_y, E_z being the electric field components of the axisymmetric NanoMi lens.

The electric field components must also be expanded via a multipole expansion (Szilagyi, 1988; Hawkes and Kasper, 2017) to calculate the aberration coefficients of the lens. For example, third-order aberration coefficients require two terms in the expansion resulting in the following set of equations for each electric field component:

$$E_x = U'(z)\frac{x}{2} - U''(z)\frac{x(x^2 + y^2)}{16} \tag{5}$$

$$E_y = U'(z)\frac{y}{2} - U''(z)\frac{y(x^2 + y^2)}{16}$$

$$E_z = -U(z) + U'(z)\frac{(x^2 + y^2)}{16}$$

This equation of motion is solved using the RK54DP method, but the position and slope of x and y are written as a DA object, using functionality provided by the differential algebra package DaceyPy (Python wrapper of DACE, 2022). By solving the equation of motion in this manner and propagating the electron ray to the image plane, a polynomial equation whose coefficients are the aberration coefficients is obtained. The following function shows how to calculate the polynomial expression that describes the particles' final coordinates as a function of input coordinates:

$$\eta \begin{bmatrix} x_f \\ x'_f \\ y_f \\ y'_f \end{bmatrix} = \sum_{\substack{i+j+k+l=\eta \\ i,j,k,l=0 \sim \eta}} x_0^i x_0'^j y_0^k y_0'^l \eta \begin{bmatrix} A_{ijkl} \\ B_{ijkl} \\ C_{ijkl} \\ D_{ijkl} \end{bmatrix} \tag{6}$$

For instance, with $\eta = 3$ placed into the above equation, one obtains a third-order polynomial expression with 35 terms comprised of all possible combinations of position and slope of each variable. The coefficients $A_{ijkl}, B_{ijkl}, C_{ijkl}$ & D_{ijkl} represent coefficients associated with each term in the polynomial expansion and correspond to a particular aberration coefficient. For instance, A_{0300} is the coefficient associated with x_0^3 , which is the spherical aberration coefficient in the x direction. Solving (4) via the DA method for a single ray trace determines the value of the coefficient of each term in this polynomial, and is a convenient method because it only requires a single ray trace to obtain aberration coefficients to any desired order.

On the other hand, the aberration integral method combines the position and slope of the principal rays g & h and the various derivatives of the axial field to create a series of integrals that we solve numerically via Simpson's rule. For each of the third-order aberration coefficients, there is a distinct aberration integral to solve (see supplementary section). The drawback of the aberration integral method is that the specific aberration integral equation must be obtained for each type of electron microscope component, and there exists a different set of equations for round lenses, electron mirrors, quadrupoles and so on. Fortunately, in the case of a round electrostatic and magnetic lens, the aberration integrals can easily be found in the literature or textbooks (Szilagyi, 1988;

Hawkes and Kasper, 2017). In the case of a round lens, aberration integrals are straightforward to solve, but in the case of more exotic components, the differential algebra method can be a convenient viable alternative to obtaining aberration coefficients, as it does not require a special derivation to obtain a new set of aberration integrals for that type of component (Liu et al., 2011; Radlička, 2019). It is important to note that each time for a new magnification (i.e. different object location before the lens), the differential algebra method or aberration integral method that calculate the real aberration coefficients must be solved again, with a new set of rays starting from the object's location.

In the case of the NanoMi lens, if the ratio of U_l/U_0 is appreciably large (equal or greater than U_l/U_0 of 0.9), then the image will be formed inside the lens field when the object is located outside the lens field, and the asymptotic aberration coefficients must be calculated instead to accurately model the lens performance. Asymptotic aberration coefficients also provide a more useful representation of the performance of the lens than the real aberration coefficients, as the asymptotic aberration coefficients can be characterised as a function of magnification in the form of a fourth-order polynomial. As a result, one can find all third-order aberrations for a given magnification of the lens by solving a single set of aberration integrals – see the section: Asymptotic Aberration Coefficients & Optimal Object Location for more information.

Fig. 5 demonstrates how the real and asymptotic spherical aberration coefficients (C_{so}) with respect to the object change for different values of U_l/U_0 . For an object initially located outside the lens field, when U_l/U_0 is 0.8 or less, the real image will always also be formed outside the lens field, and the real and asymptotic coefficients coincide. As the lens becomes stronger, and the focal length shortens, the real and asymptotic coefficients diverge. In Fig. 5, the graph of the real spherical aberration coefficients has been calculated via the DA method and the real aberration integral method, and both methods return the same real spherical aberration coefficient for a given magnification. The asymptotic spherical aberration has been calculated via the asymptotic aberration integral method (see Eqs (8), (9) and (10)). At a voltage ratio of $U_l/U_0 = 1.0$, the rays which form a real image inside the lens are bent sufficiently after forming the image, such that the real and asymptotic values of spherical aberration with respect to the object diverge drastically. It is important to note that the magnification values presented in Fig. 5 are chosen to demonstrate the ability of TEMGYM Advanced to calculate the difference between the asymptotic and real aberrations, and were calculated using object positions far enough away from the centre of the NanoMi lens (between -100m and -600m) so that the image is formed

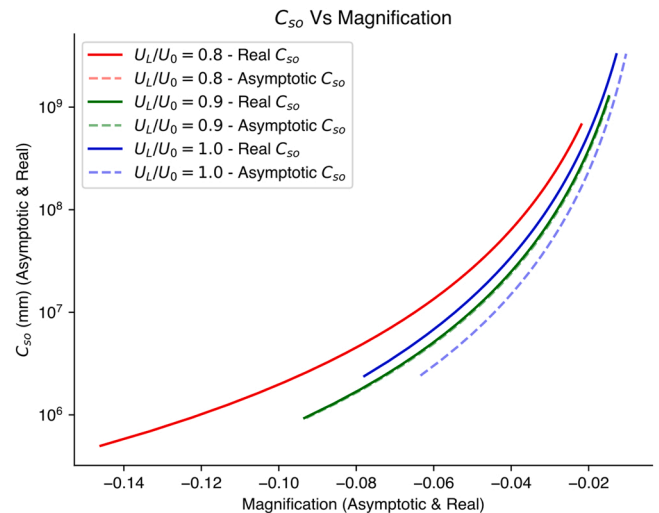


Fig. 5. Plot of real & asymptotic spherical aberration coefficients w.r.t the object, against real and asymptotic magnification. As U_l/U_0 increases, the real and asymptotic images diverge, including the aberration coefficients. The position of the object on the z -axis was varied between -100mm and -600m .

inside the lens field, and asymptotic aberrations are apparent. As the object moves closer to the lens centre, the image will be further magnified, but form outside the field of the lens, and thus the real aberrations and asymptotic aberration values will converge.

It is important to note that there are two ways to present the value of spherical aberration of the lens: With respect to the object (C_{so}), or with respect to the image (C_{si}). Typically, the spherical aberration term quoted in literature is the spherical aberration with respect to the object (C_{so}); however, it is also possible to multiply this coefficient by the magnification m of the image to determine the spherical aberration with respect to the image plane.

$$C_{si} = m \times C_{so} \quad (7)$$

Another useful metric to describe the lens performance is the size of aberration disk in the image plane, δr_{si} which is proportional to C_{si} (Szilagyi, 1988; Hawkes and Kasper, 2017). Therefore, it is important to be able to translate between the two values, and to specify which coefficient, C_{si} or C_{so} is being discussed.

In the case of U_i/U_0 of less than 0.9, either the real aberration integral method, the asymptotic aberration integral method or the differential algebra method can be used to calculate the real third-order aberration coefficients, whereas for U_i/U_0 of 0.9 or greater, only the asymptotic aberration integral method is valid to determine the aberration coefficients of the lens.

6. NanoMi lens spot diagrams

Although the DA method can only be used to calculate the real aberration coefficients, and thus it is only applicable when the lens is sufficiently weak ($U_i/U_0 < 0.9$), the polynomial expression obtained by the DA method (see Eq (7)) is convenient as the expression to obtain the location of a ray in the image plane from a new set of initial conditions in the object plane comes readily formed. Thus, one can find the position of thousands of rays in the image plane that begin with a different initial condition in the object plane, without the need to solve for a new ray path. The code to perform the differential algebra method is also shorter and more straightforward than the aberration integral method. Furthermore, obtaining fifth-order aberrations *via* the DA method is also easier, as one simply needs to add another term to the field expansion and change the order of the DA expansion to 5 instead of 3. On the other hand, calculating fifth-order aberrations *via* the aberration integral method is considerably more involved, as one needs to describe a new set of aberration integrals (Hawkes and Kasper, 2017).

Fig. 6 shows how the NanoMi lens images a series of spots in the object plane, including 3rd order geometric aberrations, and has been generated using the polynomial expression obtained *via* the DA method. Each spot in the object plane generates a cone of rays released with a semi-angle of 10mrad, and an ideal lens images a single spot from the object plane as a single spot at the image plane. The aberrations of the lens create a deformed spot whose shape depends on the aberration coefficients. Fig. 6 demonstrates how users can use our software to inspect the performance of their lens design visually, and compare how different lens designs and/or operating conditions affect the beam spot.

Fig. 7 displays how each individual aberration coefficient contributes to an aberrated beam spot. By only selecting specific terms in the aberration polynomial generated by the DA method, one can inspect how each individual aberration impacts the overall beam shape (see (Landers et al., 2023; Cheng et al., 2001)). Out of all the aberration terms, spherical aberration is the most important as it is the only aberration that does not vanish when the object is placed on the optical axis; it is dependent only on the cube of the initial beam angle. Coma is the second most crucial aberration, as it depends on the square of the initial beam angle multiplied by one position term. The subsequent aberrations are far less critical; it is possible to cancel the field curvature coefficient if the image is analysed on a curved surface tangent to the Gaussian image plane, and the effect of distortion is much weaker than each of the other aberration coefficients (Hawkes and Kasper, 2017).

7. Asymptotic aberration coefficients and optimal object location

If the voltage ratio U_i/U_0 is equivalent to 0.9 or greater, the lens forms an image inside its electrostatic field for an object located outside of it. Thus the asymptotic aberration coefficients must be calculated instead of the real aberration coefficients, and again a series of aberration integrals are solved to obtain the asymptotic aberration coefficients. The asymptotic aberration integrals can be cast into many different forms, making the computation of the coefficients easier, and the authors are aware of formulations published by published by Kuyatt et al. (1974), Orloff (2017) & Szilagyi (1988), and have found the formulation described by Orloff (2017) to be the most convenient to implement. Eq (8) displays the quartic polynomial that can calculate the asymptotic spherical aberration with respect to the object as a function of asymptotic magnification, m :

$$C_{so} = \frac{C_4}{m^4} + \frac{C_3}{m^3} + \frac{C_2}{m^2} + \frac{C_1}{m} + C_0 \quad (8)$$

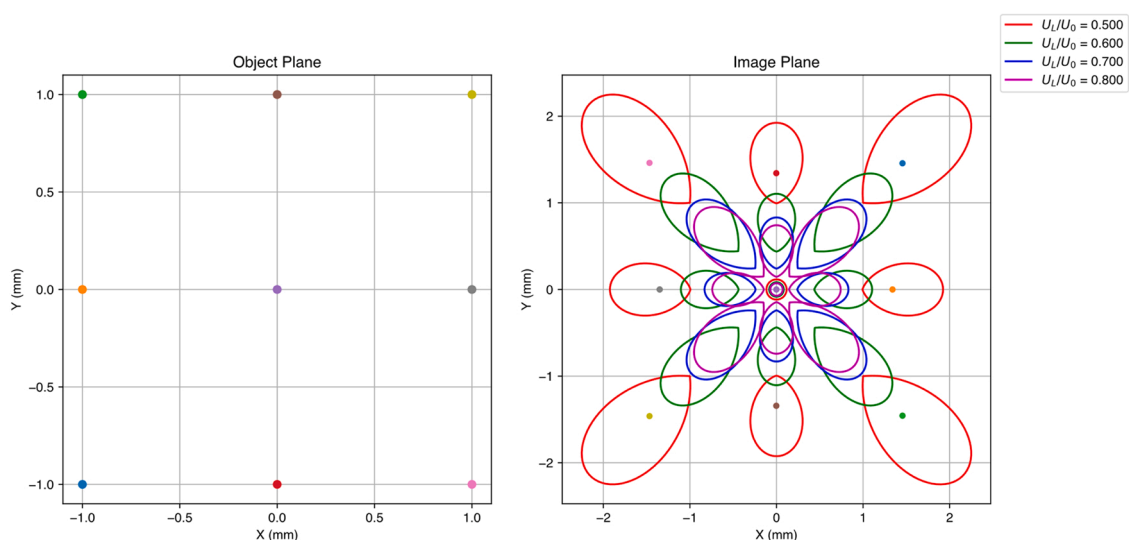


Fig. 6. Aberration diagram obtained *via* the DA method for four different voltage ratios, and nine spot positions in the object plane. The coloured dots in the image plane indicate which ray position from the object plane created the aberration spot for U_i/U_0 of 0.5.

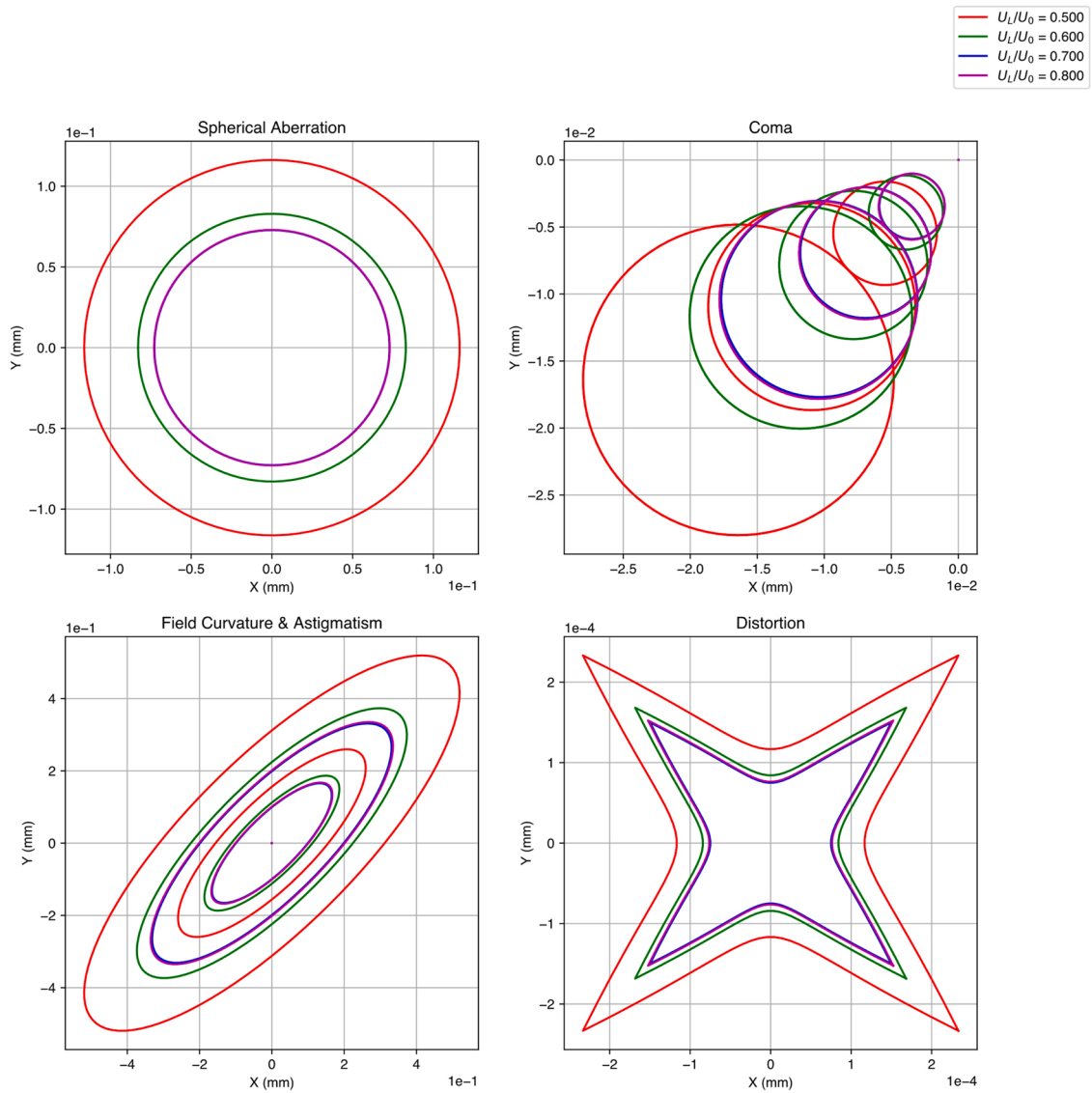


Fig. 7. Individual aberration spot diagram, obtained via the DA method for four different voltage ratios. Spherical aberration parameters: Object plane semi-angle: 10mrad. Coma parameters: Object plane semi-angle: 10mrad. Object plane radial position: 0to0.1mm. Field curvature & astigmatism parameters: Object plane semi-angle: 10mrad. Object plane radial position: 1mm. Distortion parameters: Object plane position: Square of side length 0.2mm centred about 0.

where the coefficients of Eq (8) C_4, C_3, C_2, C_1 and C_0 are given by the following expressions:

$$\begin{aligned}
 C_4 &= i_1 f_o^4 \\
 C_3 &= -4i_2 f_o^4 - r^2 f_o / 2 \\
 C_2 &= 2(i_3 + i_4) f_o^4 \\
 C_1 &= -4i_5 f_o^4 - f_o / 2 \\
 C_0 &= i_6 f_o^4
 \end{aligned}
 \tag{9}$$

where f_o and f_i are the object and image side focal lengths, and $r = \frac{f_o}{f_i}$. In a symmetric lens, $f_o = f_i$, $i_1 = i_6$, and $i_2 = i_5$, therefore only three independent coefficients are needed to characterise the asymptotic spherical aberration coefficients entirely as a function of m , C_2, C_1 and C_0 .

The values of i_n are found by solving the following set of aberration integrals:

$$\begin{aligned}
 i_1 &= \int_a^b \Lambda_e G^4 dz \\
 i_2 &= \int_a^b \Lambda_e G^3 \bar{G} dz - \frac{1}{8f_o f_i^2} \\
 i_3 &= \int_a^b \Lambda_e G^2 \bar{G}^2 dz - \frac{U_o^{1/2}}{24f_o^2} \int_a^b \frac{U'}{U^{3/2}} dz \\
 i_4 &= 2 \int_a^b \Lambda_e G^2 \bar{G}^2 dz - \frac{U_o^{1/2}}{24f_o^2} \int_a^b \frac{U'}{U^{3/2}} dz \\
 i_5 &= \int_a^b \Lambda_e G \bar{G}^3 dz - \frac{1}{8f_o^3} \\
 i_6 &= \int_a^b \Lambda_e \bar{G}^4 dz
 \end{aligned}
 \tag{10}$$

with

$$\Lambda_e = \frac{1}{64} \left(\frac{U}{U_0} \right)^{1/2} \left[4 \left(\frac{U'}{U} \right)^2 - \frac{U' U''}{U^2} - 10 \left(\frac{U'}{U} \right)^2 \frac{U'}{U} + 10 \left(\frac{U'}{U} \right)^4 \right] \quad (11)$$

where the limits a and b . represent the start and end of the potential of the lens. In the calculations shown in this work, $a = -50\text{mm}$ and $b = 50\text{mm}$, respectively. G and \bar{G} are two rays obtained again by solving Eq (1), which are incident to the lens parallel to the axis on the object and image side with the following initial conditions:

$$\lim_{z \rightarrow -\infty} G(z) = 1, \lim_{z \rightarrow \infty} \bar{G}(z) = 1 \quad (12)$$

The ray G is traced through the lens with an initial slope of 0, and an initial radial position of 1 on the axis beginning at $a = -0.05\text{m}$. Because the lens potential is centred around 0 and symmetric, G can be mirrored to obtain \bar{G} .

Table 1 displays the coefficients of the asymptotic spherical aberration polynomial for three different voltage ratios. Although the NanoMi lens is symmetric (thus $C_1 = C_3$ and $C_0 = C_4$), there is a marginal difference between each of the coefficients, which should be equivalent. The error in the fit of the potential shown in Fig. 2 can explain this, because the regression method used did not *exactly* symmetrically fit the axial potential. Nevertheless, the resulting difference in the polynomials plotted with the coefficients C_0 , C_1 and C_2 , or C_2 , C_3 and C_4 , or the average of both, is negligible.

The asymptotic aberration coefficients are advantageous because they formulate the spherical aberration values as a function of magnification via a quartic polynomial. In the case of the real aberration coefficients, a new set of rays and aberration integrals must be computed for each object position, or a new DA ray trace must be performed with the particle beginning in a new object position to obtain the real aberration coefficients.

Multiplying Eq (5) by m , creates a polynomial equation that describes how the asymptotic spherical aberration coefficient with respect to the image plane changes with the asymptotic magnification, m .

$$C_{si} = \frac{C_4}{m^3} + \frac{C_3}{m^2} + \frac{C_2}{m} + C_1 + C_0 m \quad (13)$$

The Newton-Raphson method can be used to find a root in this function's derivative, which will calculate the magnification with the smallest spherical aberration in the image plane (See (Szilagy, 1988) for more details). Fig. 8 (left panel) shows how the asymptotic spherical aberration coefficient calculated with respect to the image changes with respect to magnification. The right panel of Fig. 8 shows how object location changes with respect to magnification, and where to place the object to obtain the smallest spherical aberration in the image plane. In the case of the NanoMi Lens, our results highlight some drawbacks of electrostatic lenses. The object location for each voltage ratio (U_i/U_0) that gives the smallest spherical aberration disc in the image plane is inside the lens field. It is not recommended to immerse an object inside the field of the NanoMi Lens, as doing so would disrupt the lens's electrostatic field, unlike the magnetic lens case, which does allow an object to be placed inside the field of the lens to minimise the spherical aberration.

The spherical aberration of this same lens design was previously measured by Rempfer (1985) using an optics table. However, this

Table 1

Asymptotic spherical aberration coefficients of the NanoMi lens for different voltage ratios.

	C_0	C_1	C_2	C_3	C_4
$U_i/U_0 = 0.8$	0.14450	-0.46106	0.611484	-0.46143	0.14463
$U_i/U_0 = 0.9$	0.05537	-0.13303	0.14866	-0.13318	0.05543
$U_i/U_0 = 1.0$	0.03754	-0.01911	0.02946	-0.01908	0.03759

method of calculating asymptotic focal length and aberration coefficients was criticised by (Hawkes and Lencová, 2002), who demonstrated that the coefficients are only valid in a thin lens approximation. Rempfer (1985) measured the asymptotic C_{so} of this lens design with a U_i/U_0 of 1.0 to be approximately 50mm for an object located outside the field of the lens, and this work finds that no voltage ratio approaches this performance for any magnification. Converting the ideal C_{si} value found in Fig. 8 into C_{so} by dividing by the magnification, C_{so} is still at best $\sim 72\text{mm}$ for $U_i/U_0 = 1.0$ and this also corresponds to the case when the object is located 6 mm away from the centre of the lens, which is not possible due to the drawbacks of symmetric lens design. The NanoMi project has accounted for this design flaw and created an "asymmetric" lens design that allows object placement within less than 11mm of the centre electrode. It is thus much better to use the asymmetric lens as an imaging lens, rather than the symmetric lens design studied in this work, and to only use the symmetric lens as a condenser lens within the microscope system.

8. Conclusion

The methods presented in this work demonstrate an open-source platform that can characterise the properties of real electrostatic lens designs. This aspect of the software TEMGYM Advanced has been developed to demonstrate how a set of open-source tools and methods can be used to model a real microscope lens, which is a necessary step towards the creation of an electron microscope digital twin. Commercial software that performs the same analysis have been developed over many decades and are far more mature in terms of the features and capabilities of the software, and TEMGYM Advanced as a new offering in this domain has many features and capabilities to add and expand upon. The software presented in this work shows how to generate a complete picture of the performance of a lens design, in terms of its focal length and aberration coefficients, and it allows lens designers to understand how the spherical aberration, which is one of the primary limiters of performance, changes as a function of magnification for a specific lens design.

Future work will focus on implementing the ability to calculate fifth-order geometric and chromatic aberration coefficients, and the ability to characterise more components, such as multipole elements, electron mirrors, and other exotic components that create today's high-performing instruments. It may also be interesting to explore if the differential algebra method can calculate asymptotic aberration coefficients, as this would avoid the need to find or derive aberration integrals for each type of component.

Furthermore, this work did not apply the parallelised ray-tracing capabilities of TEMGYM Advanced to the NanoMi Lens (see Landers et al., 2023). In future work, with full access to the 3D CAD model of the entire NanoMi microscope, TEMGYM Advanced can implement a complete digital twin and apply the parallelised ray tracing code to the entire instrument, provided 3D FEM methods can also be used to obtain the field of the stigmator and dipole deflectors inside the microscope. All code and methods are accessible on the associated GitHub repository (Advanced, 2023), which should be a valuable resource to electron microscopists who wish to learn how to analyse their lens designs.

Declaration of Competing Interest

The authors declare that they have no known competing financial interests or personal relationships that could have appeared to influence the work reported in this paper.

Data Availability

No data was used for the research described in the article. Code is available on the corresponding GitHub: <https://github.com/AMCLab/TEMGYMAAdvanced>.

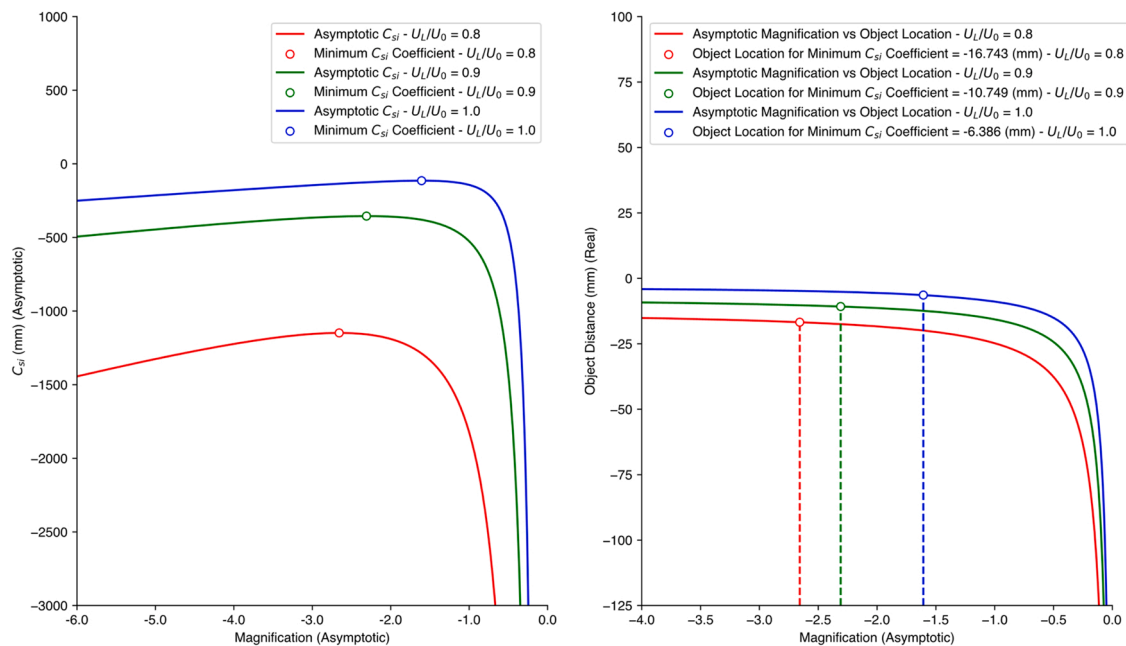


Fig. 8. Left panel plots C_{si} as a function of asymptotic magnification for three different values of U_i/U_0 , calculated via Eq (8). The circular dot denotes the magnification that gives the smallest C_{si} . The right panel plots asymptotic magnification vs real object location. Again the circular dot corresponds to the asymptotic magnification (and thus real object location) that gives the smallest values of C_{si} .

Acknowledgements

The research was supported by the Irish Research Council EPSPG/2019/509 and the Ernst Ruska-Centre for Microscopy and Spectroscopy with Electrons (ER-C). We would like to thank the NanoMi project for access to the CAD drawings of the lenses.

References

- 3D CAD Software & Product Development Platform | Onshape. Available at: ([https://www.onshape.com/en/platform?utm_source=google&utm_medium=cpc&utm_campaign=Google_Search_EMEA&utm_content=\[UK_Generic_PMax\]_EN&utm_term=&mostrecentleadsources=google-cpc-](https://www.onshape.com/en/platform?utm_source=google&utm_medium=cpc&utm_campaign=Google_Search_EMEA&utm_content=[UK_Generic_PMax]_EN&utm_term=&mostrecentleadsources=google-cpc-)). (Accessed: 21st January 2023).
- AMCLab/TEMGYMAdvanced. Available at: (<https://github.com/AMCLab/TEMGYMAdvanced>). (Accessed: 3rd February 2023).
- Baltzis, K.B., 2008. The FEMM package: a simple, fast, and accurate open source electromagnetic tool in science and engineering. *J. Eng. Sci. Technol. Rev.* 1, 83–89.
- Bellemare, M.G., et al., 2020. Autonomous navigation of stratospheric balloons using reinforcement learning. *Nat* 2020 5887836 588, 77–82.
- Bertoni, G., et al., 2023. Near-real-time diagnosis of electron optical phase aberrations in scanning transmission electron microscopy using an artificial neural network. *Ultramicroscopy* 245, 113663.
- Berz, M., 1989. Differential algebraic description of beam dynamics to very high orders. *Science* 24, 109–124.
- Cheng, M., Tang, T., Yao, Z., 2001. Study on differential algebraic chromatic aberration method for Glaser's bell-shaped magnetic lenses. *Opt* 112, 483–486.
- Clausen, A., et al., 2020. LiberTEM: Software platform for scalable multidimensional data processing in transmission electron microscopy. *J. Open Source Softw.* 5, 2006.
- COMSOL. COMSOL. 2020.
- De La Peña, F. et al. hyperspy/hyperspy: Release v1.6.5. *zndo* 2021. doi:10.5281/ZENODO.5608741.
- Degrave, J., et al., 2022. Magnetic control of tokamak plasmas through deep reinforcement learning. 414 | *Nat* | 602.
- Devi, K.U., Sanavullah, M.Y., 2011. Performance analysis of exterior(outer) rotor permanent magnet brushless DC (ERPMBLDC) motor by finite element method. *ICECT 2011 - 2011 3rd Int. Conf. Electron. Comput. Technol.* 3, 426–430.
- A. Dormand Prince solver for ordinary differential equations (odes) of the first order. Digital explorations. Available at: (<https://web.archive.org/web/20150907215914/http://adorio-research.org/wordpress/?p=6565>). (Accessed: 21st January 2023).
- Dormand, J.R., Prince, P.J., 1980. A family of embedded Runge-Kutta formulae. *J. Comput. Appl. Math.* 6, 19–26.
- Dupuy, J. Contrôle dynamique et optimisation des observations en microscopie électronique en transmission. (Université Paul Sabatier - Toulouse III, 2021).
- Dyck, O., Jesse, S., Kalinin, S.V., 2019. A self-driving microscope and the Atomic Forge. *MRS Bull.* 44, 669–670.
- El-Kareh, A. Electron beams, lenses, and optics. , 2012.

- giovannipurpura/dacey: Python wrapper of DACE, the Differential Algebra Computational Toolbox. Available at: (<https://github.com/giovannipurpura/dacey>). (Accessed: 21st December 2022).
- Graef, M.De, 2003. Introduction to conventional transmission electron microscopy. *Introd. Conv. Transm. Electron Microsc.* <https://doi.org/10.1017/CBO9780511615092>.
- Hawkes, P. & Kasper, E. Principles of Electron Optics, Volume 1: Basic Geometrical Optics. Principles of Electron Optics, Volume 1: Basic Geometrical Optics (2017). doi:10.1016/C2015-0-06652-7.
- Hawkes, P.W., Lencová, B., 2002. Studies on the asymptotic cardinal elements and aberration coefficients of symmetric unipotential electrostatic lenses. *Opt. (Stuttg.)* 113, 78–82.
- Johnstone, D.N. et al. pyxem/pyxem: pyxem 0.10.0. , 2019). doi:10.5281/ZENODO.3533653.
- Kalinin, S.V., et al., 2021. Automated and autonomous experiments in electron and scanning probe microscopy. *ACS Nano* 15, 12604–12627.
- Kang, Y., Liu, X., Zhao, J., Tang, T., 2017. High order aberrations calculation of a hexapole corrector using a differential algebra method. *Nucl. Instrum. Methods Phys. Res. Sect. A Accel. Spectrometers, Detect. Assoc. Equip.* 846, 8–12.
- Komárek, J., Klogner, V., 2022. Design of electromagnetic control of the needle gripping mechanism. *Mach.* 2022, Vol. 10, Page 309 10, 309.
- Koster, A.J., de Ruijter, W.J., 1992. Practical autoalignment of transmission electron microscopes. *Ultramicroscopy* 40, 89–107.
- Kuyatt, C.E., Dichio, D., Natali, S.V., 1974. Cite as. *Rev. Sci. Instrum.* 45, 2331.
- Landers, D., Clancy, I., Dunin-Borkowski, R.E., Weber, D., Stewart, A. TEMGYM Advanced: Software for Electron Lens Aberrations and Parallelised Electron Ray Tracing. *Ultramicroscopy* (2023).
- Lencová, B., Zlámal, J., 2008. A new program for the design of electron microscopes. *Phys. Procedia* 1, 315–324.
- Liu, H., Wang, L., Rouse, J., Munro, E., 2011. Design and optimization of multipole lens and Wien filter systems. *Nucl. Instrum. Methods Phys. Res. Sect. A Accel. Spectrometers, Detect. Assoc. Equip.* 645, 300–306.
- Makino, K., Berz, M., 2006. COSY INFINITY Version 9. *Nucl. Instrum. Methods Phys. Res. Sect. A Accel. Spectrometers, Detect. Assoc. Equip.* 558, 346–350.
- Malac, M., et al., 2022. NanoMi: An open source electron microscope hardware and software platform. *Micron* 163, 103362.
- Munro, E. Computer-aided-design methods in electron optics. (1972).
- Munro, E., 2011. Numerical simulation methods for electron and ion optics. *Nucl. Instrum. Methods Phys. Res. Sect. A Accel. Spectrometers, Detect. Assoc. Equip.* 645, 266–272.
- Olszta, M. et al. An Automated Scanning Transmission Electron Microscope Guided by Sparse Data Analytics. doi:10.1017/S1431927622012065.
- Orloff, J. Handbook of charged particle optics, second edition. Handbook of Charged Particle Optics, Second Edition (CRC Press, 2017). doi:10.1201/9781420045550.
- Radlička, T., 2019. Correction of parasitic aberrations of hexapole corrector using differential algebra method. *Ultramicroscopy* 204, 81–90.
- Rempfer, G.F., 1985. Unipotential electrostatic lenses: Paraxial properties and aberrations of focal length and focal point. *J. Appl. Phys.* 57, 2385.
- Robitaille, T.P., et al., 2013. Astropy: a community python package for astronomy. *Astron. Astrophys.* 558, A33.

- Rosi, P., et al., 2022. Automatic alignment of an orbital angular momentum sorter in a transmission electron microscope using a convolutional neural network. *Microsc. Microanal.* 1–9. <https://doi.org/10.1017/S143192762201248X>.
- Rotunno, E., Grillo, V., 2022. Artificial neural network for automatic alignment of electron optical devices. *Microsc. Micro* 28.
- Shewchuk, J.R. Triangle, 1996. Engineering a 2D quality mesh generator and delaunay triangulator. in: *Lect. Notes Comput. Sci. (Incl. Subser. Lect. Notes Artif. Intell. Lect. Notes Bioinforma.)* 1148, 203–222.
- Spurgeon, S.R., et al., 2020. Towards data-driven next-generation transmission electron microscopy. *Nat. Mater.* 20, 274–279.
- Szilagy, M., 1988. Motion of charged particles in electric and magnetic fields. *Electron Ion.-. Opt.* 13–50. https://doi.org/10.1007/978-1-4613-0923-9_2.
- Tejada, A., den Dekker, A.J., Van den Broek, W., 2011. Introducing measure-by-wire, the systematic use of systems and control theory in transmission electron microscopy. *Ultramicroscopy* 111, 1581–1591.
- Tejada, A., Van Den Broek, W., Den Dekker, A.J., 2013. Measure-by-wire (MBW): an automatic control framework for high-throughput transmission electron microscopy. in (Academic Press Inc.,). *Adv. Imaging Electron Phys.* 179, 291–346 (Academic Press Inc.,).
- Vinyals, O., et al., 2019. Grandmaster level in StarCraft II using multi-agent reinforcement learning. *Nature* 575, 350–354.
- Wang, L., 2004. Simulation of electron optical systems by differential algebraic method combined with Hermite fitting for practical lens fields. *Microelectron. Eng.* 73–74, 90–96.
- Wurman, P.R., et al., 2022. Outracing champion Gran Turismo drivers with deep reinforcement learning. *Nat* 2022 6027896 602, 223–228.
- Xu, M., Kumar, A., LeBeau, J.M., 2022. Towards augmented microscopy with reinforcement learning-enhanced workflows. *Microsc. Micro* 28, 1952–1960.